Acta Crystallographica Section A
Foundations of Crystallography
ISSN 0108-7673

Received 25 May 1999
Accepted 20 August 1999

Atoms in crystals – from experimental charge densities

Claus Flensburg[a]* and Dennis Madsen[b]

[a]Centre for Crystallographic Studies, Department of Chemistry, University of Copenhagen, Universitetsparken 5, DK-2100 Copenhagen, Denmark, and [b]ESRF, BP 220, F-38043 Grenoble CEDEX, France. Correspondence e-mail: claus@ccs.ki.ku.dk

An implementation is described of R. F. W. Bader's [*Atoms in Molecules: a Quantum Theory* (1990). Oxford: Clarendon Press] virial fragmentation of the electron density as applied to experimentally determined electron densities. It is analogous to the *PROMEGA* method [Keith (1993), PhD thesis, McMaster University, Ontario, Canada]. Integrated atomic properties have been determined using the models from two recent accurate charge-density studies: methylammonium hydrogen succinate monohydrate and methylammonium hydrogen maleate.

1. Introduction

Several schemes to define 'atomic' charges have been proposed (Hirshfeld, 1977; Mulliken, 1955; Bader, 1990; Spackman & Byrom, 1996), some of which have been used in experimental electron-density studies. Meister & Schwarz (1994) give an extended survey of atomic charge definitions. Generally, the methods can be divided into two distinct classes based on the boundary type of the atoms, *i.e.* fuzzy or discrete boundaries.

Bader's quantum theory of atoms in molecules (QTAM) (Bader, 1990) is a well established tool to characterize electron densities derived from theoretical calculations. It can readily be extended to cover three-dimensionally periodic electron densities (Zou & Bader, 1994; Tsirelson *et al.*, 1995).

Using the definition of a virial fragment to partition an electron density, the concept of an atom emerges where discrete boundaries separate the atoms. This definition is firmly based on quantum-mechanical methods. Recently, the QTAM has been successfully applied to experimentally determined electron densities derived from X-ray single-crystal diffraction data (Flensburg *et al.*, 1995; Howard *et al.*, 1995; Bianchi *et al.*, 1996; Espinosa *et al.*, 1996; Roversi *et al.*, 1996; Koritsánszky *et al.*, 1998; Madsen, Flensburg & Larsen, 1998; Madsen, Iversen *et al.*, 1998). These analyses have been based on the location and characterization of critical points $[\nabla\rho(\mathbf{r}_c) = 0]$ for intramolecular and hydrogen-bond interactions in the electron density.

The previous implementations of Bader's partitioning scheme have been applied to molecular (Biegler-König *et al.*, 1982; Stefanov & Cioslowski, 1995; Popelier, 1994) and periodic *ab initio* calculations (Gatti *et al.*, 1994). None of these implementations have been applied to experimentally determined electron densities – wherefore we decided to implement Bader's partitioning scheme in the *VALRAY* program (Stewart *et al.*, 1998).

This implementation is conceptually based on the algorithm called *PROMEGA*, which was first proposed by Keith (1993) and has recently been described in detail by Popelier (1998).

In *VALRAY*, the rigid pseudo-atom model of Stewart (1976) is used to model the charge density in the crystallographic unit cell.

The underlying assumption is that only pure kinematic or dynamic X-ray scattering gives rise to the measuring of photons at the detector. Other physical interactions should be eliminated/corrected for before the modelling of the electron density takes place. Deconvolution of the electron and the nuclear density distributions is another approximation of this model. The electron density of an atom follows rigidly (*i.e.* without distortion) the nuclear position.

It should be emphasized that the static electron density determined from X-ray diffraction methods is not a quantum object but rather, as described by R. F. Stewart (1991), 'the ghost of a quantum object'. It is therefore interesting to elucidate any differences between results of the Bader partitioning obtained from *ab initio* and experimentally determined charge densities, respectively. Current research (Flensburg & Gatti, 1997, 1999) indicates that there is excellent agreement between atomic properties determined from theoretical and experimentally determined electron densities. Obtaining atomic properties from experimentally determined electron densities is therefore a viable route, especially for characterizing intermolecular interactions.

In this work, we present a topological analysis where the boundaries of the gradient field are determined and a subsequent integration over the atomic basins is performed.

Table 1
Global errors of the integrations of MAHS and MADMA.

Compound	$N^{\rm err}$(%)	$V^{\rm err}$(%)	$L^{\rm err}$(10^{-3} e Å^{-2})
MAHS	−0.05	−0.25	2.2
MADMA	−0.07	−0.38	5.9

2. Description of the algorithm

The algorithm is based on two properties of the atomic basin: (i) The interatomic surface (IAS) is never crossed by a gradient path (of the electron density – hereafter in short 'gradient path'); (ii) all gradient paths terminate at an attractor – except for gradient paths lying in the surface, which terminate at bond or ring critical points.[1] Using these properties, a set of points arbitrarily close to the IAS can be determined.

A set of rays emanating from the attractor is constructed in a spherical-polar coordinate system so that the rays in each θ plane on the unit sphere have the same $\Delta\varphi$ separation. The integration thereby becomes less dependent on the choice of coordinate system (more 'rotationally invariant'), which is not the case if a standard division is chosen. A standard division of the θ, φ grid into an equal number of φ points for each θ plane will yield a more dense concentration of integration points near the poles, *i.e.* for $\theta \approx \{0, \pi\}$.

Points in the direction of a given ray at various distances from the attractor are used to determine the intersection of the ray with the IAS. See Fig. 1. When the starting point of the ray is inside the atomic basin belonging to the attractor, a trace along the gradient will terminate at the attractor itself. When the starting point of the ray is on the other side of the intersection of the IAS, the trace along the gradient will terminate at another attractor.

In the direction of a given ray, the distance of the first point is chosen as 0.8 times the length of the previous ray (the distance from the attractor to the IAS). This was found empirically to give the most efficient implementation. If the first point on a ray is found to be outside the basin of the attractor, the length is set to a preset value by the user (a so-called β sphere). That value is also used for the very first ray. The next starting point, in the direction of a given ray, from which the gradient is traced, is given by a constant increment until the IAS is crossed. In that case, the increment is halved. This is repeated until the increment is below a given threshold (typically 10^{-4} Å).

Our implementation does not take into account that rays emanating from the attractor may have multiple intersections with the IAS. In the systems investigated so far, summations of the integrated atomic volumes have been very close to the unit-cell volume, indicating that this simplification of the algorithm is acceptable in most cases (*cf.* §3.2).

Given the set of points arbitrarily close to the IAS, several properties can be determined by performing an integration over the atomic basin. The three-dimensional integration is divided into three one-dimensional integrations, two angular and one radial. In the two angular dimensions (θ, φ), a trapezoidal integration technique is used while a Gauss–Legendre integration method (Press *et al.*, 1988) is used for the radial dimension. With the software, we are at present able to compute the following integrated properties: volume, Laplacian, charge, and each component of the dipole moment and quadrupole moments,[2] respectively. This can of course be extended to enable the computation of any atomic property depending on the electron density or its derivatives.

As an estimate of the accuracy of the IAS determination and the integration, three measures can be used. Firstly, the total number of electrons in the unit cell, $F(000)$, is known. Secondly, the unit-cell volume is known and, finally, the integrated Laplacian of each basin should be zero (Bader, 1990). For the number of electrons and the total volume, we use the error definitions:

$$N^{\rm err} = \sum_{\Omega} m_{\Omega} N_{\Omega} - N_{\rm cell} \Big/ N_{\rm cell}$$

$$V^{\rm err} = \sum_{\Omega} m_{\Omega} V_{\Omega} - V_{\rm cell} \Big/ V_{\rm cell},$$

where m_{Ω} is the site multiplicity for atom Ω and for the integrated Laplacian:

$$L^{\rm err} = \left(\sum_{\Omega} L_{\Omega}^2 \Big/ N_{\rm atoms} \right)^{1/2}.$$

Errors in the order of 0.01 and 0.1% for the number of electrons and the volume, respectively, are usually obtained for molecular systems. $L^{\rm err}$ is generally about 3×10^{-3} e Å^{-2}. The integrated outer moments of the atoms can also be used to validate the IAS determination and subsequent integration since they have to exhibit the site symmetry of the atoms; *e.g.*, for an atom in a mirror plane, the dipole-moment-component perpendicular to the mirror plane must be zero.

3. Examples

High-resolution charge-density studies based on X-ray and neutron diffraction data have recently been carried out on two dicarboxylic acid salts of the methylammonium ion, methylammonium deuterium maleate (MADMA) (Madsen, Flensburg & Larsen, 1998) and methylammonium hydrogen succinate monohydrate (MAHS) (Flensburg *et al.*, 1995). The labelling scheme of the two compounds is shown in Fig. 2.

There is a wide variety of strong and weak inter- and intramolecular interactions in the two structures. In both salts, all possible donor atoms are involved in hydrogen bonds, linking the entities in such a way that the anions and the cations form alternating layers. In MADMA, there are two strong symmetric intramolecular O—H—O hydrogen bonds and in MAHS there is one strong symmetric intermolecular O—H—O hydrogen bond. The N—H···O interactions in both

[1] For a description of the different types of critical points in the electron density, see *e.g.* Bader (1990).

[2] Buckingham's definition of the quadrupole moment is used. This can be transformed to the traceless second-moment radial tensor (Spackman, 1992).

structures have N—O distances of 2.7–2.9 Å. The O atom in the water molecule of MAHS participates in O—H···O hydrogen bonds.

3.1. Determination of the IAS

The electron density at a given point is calculated as the contributions from all pseudo-atoms within a radius of a cut-off limit. For the present calculations, a cut-off of 7 Å was used. The CPU time used for both the IAS determination and integration varies from 1/2 hour upwards per atom on a Silicon Graphics Challenge R10000 computer. The CPU time depends on the required integration accuracy and the complexity of the system, *e.g.* the number of atoms in the unit cell and the irregularity of the shape of the IASs. The determination of the IAS is the time-consuming part of the algorithm. All the determined atomic properties are therefore integrated at the same time. In the examples given here, the surfaces were determined with 48 θ planes yielding a set of 2788 points on each IAS. We used between 64 and 192 radial divisions giving between 200k and 535k integration points per atom. Using this number of integration points and strict requirements for the IAS determinations, the CPU time per atom used to calculate the results for MAHS and MADMA varied from 10 to 20 h.

3.2. Integration of atomic basins

A summation of the volumes and electron populations for the unit cell gave V_c and $F(000)$ within 0.4 and 0.1%, respectively, in both compounds. The integrated Laplacian was of the order of 10^{-2} e Å^{-2} for all types of atoms with the chosen level of accuracy, giving $L^{\rm err}$ about 3×10^{-3} e Å^{-2} in both cases. The global error measures are given in Table 1. These values are similar to those reported for *ab initio* calculations. Thus, we are confident that the IASs have been determined with high precision and the integrations are reliable. Some integrated properties for the atomic basins in MADMA and the cation in MAHS have already been published (Madsen, Flensburg & Larsen, 1998). The remaining results are listed in Table 2.

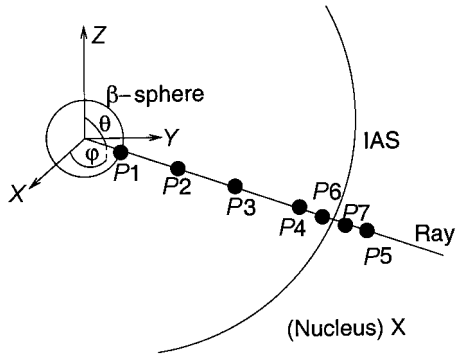

Figure 1
Coordinate system and β sphere of an atom. The integration ray is shown with seven probe points starting from the β sphere stepping outwards to point 5 where the IAS has been crossed. The step length is halved and the direction of propagation is reversed. This is repeated at point 6.

Table 2
Integrated charge (q), volume (V) and Laplacian (L) of some of the atomic basins in MAHS and MADMA.

Ω	q(Ω) (e)	V(Ω) (Å^3)	L(Ω) (10^{-3}e Å^{-2})
MAHS			
C(1)	1.45	5.4	−1.2
C(2)	−0.06	8.9	−2.0
O(1)	−1.31	16.6	−1.5
O(2)	−1.15	16.3	−1.9
H(1)	0.69	1.0	−1.9
H(2)	0.11	6.0	−1.5
H(3)	0.11	7.5	−2.0
Σ(COO^-)	−1.01	38.3	
Σ(CH_2)	0.16	22.3	
Σ(anion)	−1.02	122.3	
O(3)	−1.27	22.3	2.8
H(8)	0.66	1.5	−4.4
Σ(H_2O)	0.06	25.5	
MADMA			
C(1)	1.23	5.9	−3.1
C(2)	−0.11	12.5	−2.9
O(1)	−1.00	17.1	3.9
O(2)	−1.04	18.0	1.8
H(2)	0.14	6.2	6.5
D(2)	0.66	1.0	7.1
Σ(COO^-)	−0.81	41.0	
Σ(CH)	0.03	18.7	
Σ(anion1)	−0.90	120.4	
C(3)	1.27	5.7	−2.9
C(4)	−0.11	12.0	−3.3
O(3)	−0.98	17.6	2.2
O(4)	−1.03	16.4	1.7
H(4)	0.13	6.0	7.2
D(4)	0.71	0.9	6.9
Σ(COO^-)	−0.74	39.7	
Σ(CH)	0.02	18.0	
Σ(anion2)	−0.73	116.3	

3.2.1. Charges. Some basic properties of the charges obtained from the IAS partitioning were demonstrated in a previous paper (Madsen, Flensburg & Larsen, 1998). The QTAM partitioning leads to a larger charge transfer between the atoms than a summation of monopole populations, but the charges of the whole fragments in the two partitioning schemes are identical within the uncertainty. It was inferred that transferability is applicable to the charges of chemically equivalent basins, chemical functional groups and of the whole fragments between different crystal structures. These conclusions are underlined with the properties listed in Table 2.

3.2.2. Dipole moments. The dipole moment of the water molecule in MAHS has been calculated. Listed in Table 3 are the components and magnitude of the dipole moment calculated by two partitioning schemes: (I) Using the monopole and dipole population parameters from the multipole model; (II) using the integrated properties (charge and atomic dipoles) from the QTAM partitioning. The results from the two partitioning schemes are in excellent agreement. The monopole and dipole population parameters give an exact answer for the dipole moment for the multipole model. This is, however, only the case if there is negligible correlation with

Table 3
Dipole moment of the water molecule in MAHS as calculated by the pseudo-atom population parameters (Pop) and by QTAM partitioning.

The orientation of the dipole moments is with respect to the multipole coordinate system: **x**||**a**, **y**||**b** and **z**||**c***. The origin for these calculations is at the centre of mass for the water molecule. Standard uncertainties are in parentheses.

Type	q (e)	μ_1 (e Å)	μ_2 (e Å)	μ_3 (e Å)	$\|\mu\|$ (e Å)	$\|\mu\|$ (10^{-30} C m)
Pop	0.081 (22)	0.102 (14)	0.000 (16)	0.484 (14)	0.494 (14)	7.92 (23)
QTAM	0.059	0.099	0.00001	0.501	0.511	8.18

the other atoms in the structure. The excellent agreement of the two partitioning schemes is in this case a verification of that assumption. The integration gives furthermore a result reflecting the *m* site symmetry of the water molecule (μ_2 is close to zero). Both results agree well with other determinations of the dipole moment of water determined from diffraction and other techniques (Spackman, 1992; Espinosa *et al.*, 1996). The IASs of O(3) and H(8) are displayed in Fig. 3. Since the water molecule lies in a mirror plane, only one H atom is displayed, allowing a better view of the IAS that is shared by the O(3) atom and the symmetry-equivalent H(8′) atom, which is not shown. The IASs are colour-coded by the electrostatic potential in the crystal (Stewart, 1982). The colours reflect the direction of the dipole moment, with the O(3) end having a lower electrostatic potential than the H(8) and H(8′) end.

3.2.3. Error estimates of integrated properties. The integrated properties will be slightly biased by the actual modelling of the pseudo-atoms, *i.e.* the properties from an IAM are different from those obtained from a full multipole model. This is similar to the bias from using different levels of basis set found in quantum-chemical calculations. Despite this, we find a conservative estimate of the uncertainty in the integrated properties to be *ca* 5%. This estimate of the uncertainty is based on tests with different integration parameters and different crystallographic models.

4. Conclusions

We have successfully implemented the QTAM partitioning of the electron density for experimentally determined charge densities in the program *VALRAY*. Physically meaningful properties are determined by integration over the atomic basins.

We find that the current results are encouraging for further investigations on using the QTAM partitioning to extract experimentally determined atomic properties as an alternative to other partitioning schemes.

We thank Dr Carlo Gatti for valuable discussions. Comments on the manuscript from Professor Sine Larsen and Mr Henrik Birkedal are very much appreciated.

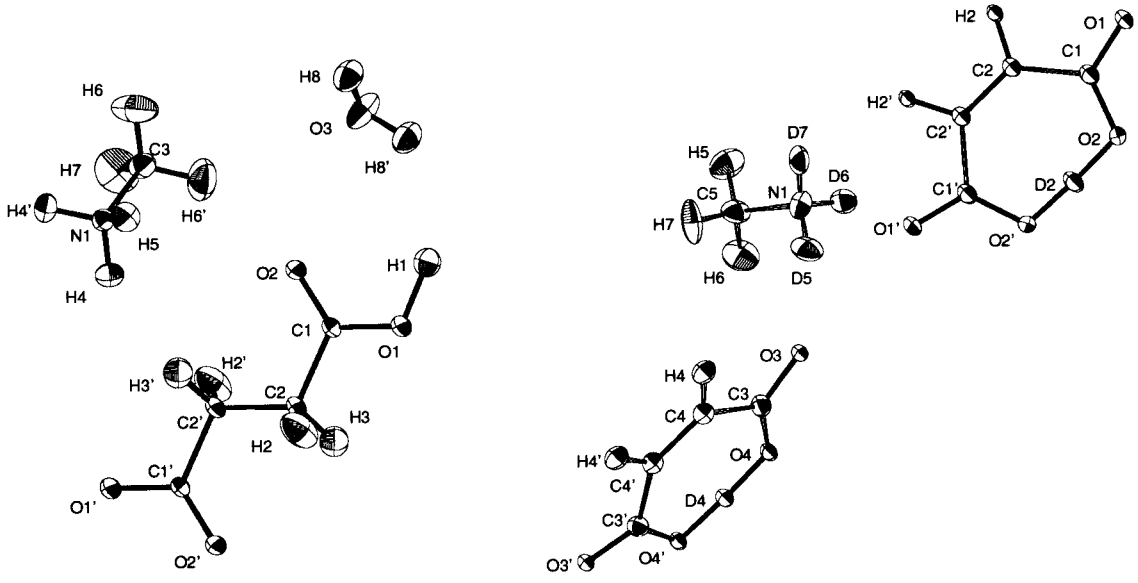

Figure 2
ORTEP (Johnson, 1976) drawings showing the labelling scheme of the entities in MAHS (left) and MADMA. Ellipsoids are drawn at the 50% probability level.

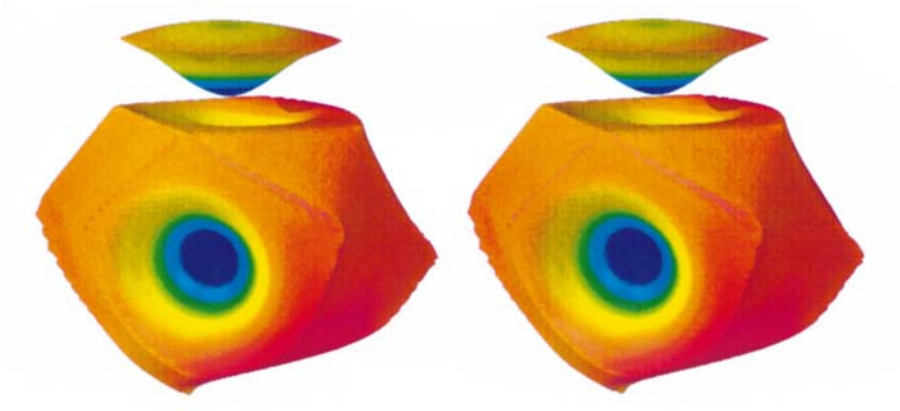

Figure 3
Stereo drawing (Merritt & Bacon, 1997) of the IASs for O(3) and H(8) in MAHS. The H(8) fragment is translated 0.75 Å away from O(3) along the O(3)—H(8) interaction line. The depression on the front side of O(3) is the IAS shared with the symmetry-equivalent H(8′) atom. The IASs are colour-coded by the electrostatic potential in the crystal. Colours range from red (−555 kJ mol^{-1}) over green (0 kJ mol^{-1}) to blue (+1111 kJ mol^{-1}).

References

Bader, R. F. W. (1990). *Atoms in Molecules: a Quantum Theory*. Oxford: Clarendon Press.

Bianchi, R., Gatti, C., Adovasio, V. & Nardelli, M. (1996). *Acta Cryst.* B**52**, 471–478.

Biegler-König, F. W., Bader, R. F. W. & Tang, T.-H. (1982). *J. Comput. Chem.* **3**, 317–328.

Espinosa, E., Lecomte, C., Molins, E., Veintemillas, S., Coussin, A. & Paulus, W. (1996). *Acta Cryst.* B**52**, 519–534.

Flensburg, C. & Gatti, C. (1997). American Crystallographic Meeting, St Louis, MO, USA.

Flensburg, C. & Gatti, C. (1999). In preparation.

Flensburg, C., Larsen, S. & Stewart, R. F. (1995). *J. Phys. Chem.* **99**, 10130–10141.

Gatti, C., Saunders, V. R. & Roetti, C. (1994). *J. Chem. Phys.* **101**, 10686–10696.

Hirshfeld, F. L. (1977). *Theor. Chim. Acta*, **44**, 128–139.

Howard, S. T., Hursthouse, M. B., Lehmann, C. W. & Poyner, E. A. (1995). *Acta Cryst.* B**51**, 328–337.

Johnson, C. K. (1976). *ORTEP-II. A Program for Plotting Thermal Ellipsoids.* Tech. Rep. ORNL-5138. Oak Ridge National Laboratory, Tennessee, USA.

Keith, T. A. (1993). PhD thesis, McMaster University, Ontario, Canada.

Koritsánszky, T., Flaig, R., Zobel, D., Krane, H.-G., Morgenroth, W. & Luger, P. (1998). *Science*, **279**, 356–358.

Madsen, D., Flensburg, C. & Larsen, S. (1998). *J. Phys. Chem.* A**102**, 2177–2188.

Madsen, G. K. H., Iversen, B. B., Larsen, F. K., Kapon, M., Reisner, G. M. & Herbstein, F. H. (1998). *J. Am. Chem. Soc.* **120**, 10040–10045.

Meister, J. & Schwarz, W. H. E. (1994). *J. Phys. Chem.* **98**, 8245–8252.

Merritt, E. A. & Bacon, D. J. (1997). *Methods Enzymol.* B**277**, 505–524.

Mulliken, R. S. (1955). *J. Chem. Phys.* **23**, 1833–1840.

Popelier, P. L. A. (1994). *Theor. Chim. Acta*, **87**, 465–476.

Popelier, P. L. A. (1998). *Comput. Phys. Commun.* **108**, 180–190.

Press, W. H., Flannery, B. P., Teukolsky, S. A. & Vetterling, W. T. (1988). *Numerical Recipes: the Art of Scientific Computing*. Cambridge University Press.

Roversi, P., Barzahgi, M., Merati, F. & Destro, R. (1996). *Can. J. Chem.* **74**, 1145–1161.

Spackman, M. A. (1992). *Chem. Rev.* **92**, 1769–1797.

Spackman, M. A. & Byrom, P. G. (1996). *Acta Cryst.* B**52**, 1023–1035.

Stefanov, B. B. & Cioslowski, J. (1995). *J. Comput. Chem.* **16**, 1394–1404.

Stewart, R. F. (1976). *Acta Cryst.* A**32**, 565–574.

Stewart, R. F. (1982). *God. Jugosl. Cent. Kristalogr.* **17**, 1–24.

Stewart, R. F. (1991). *The Application of Charge Density Research to Chemistry and Drug Design*, edited by G. A. Jeffrey & J. F. Piniella, pp. 63–101. New York: Plenum Press.

Stewart, R. F., Spackman, M. A. & Flensburg, C. (1998). *VALRAY98 Users Manual.* Carnegie Mellon University, Pittsburgh, USA, and University of Copenhagen, Denmark.

Tsirelson, V. G., Zou, P. F., Tang, T.-H. & Bader, R. F. W. (1995). *Acta Cryst.* A**51**, 143–153.

Zou, P. F. & Bader, R. F. W. (1994). *Acta Cryst.* A**50**, 714–725.